

URANS SIMULATIONS OF STATIC DRIFT AND DYNAMIC MANOUVERES OF THE KVLCC2 TANKER

S.R. Turnock (University of Southampton, Highfield, Southampton SO17 1BJ, UK)
A.B. Phillips (University of Southampton, Highfield, Southampton SO17 1BJ, UK)
M. Furlong (National Oceanography Centre, Southampton, SO14 3ZH, UK)

1 SUMMARY

Computational Fluid Dynamics is used to investigate the global forces and moments acting on the KVLCC2 hull form under going straight line, drift and pure sway planar motion mechanism tests. Simulated results are compared with experimental results for the unappended hull in shallow water and a fully appended hull with a propeller acting at the ship self propulsion point. A body fitted mesh undergoes transverse motion within an overall fixed mesh to capture planar motion mechanism tests.

A blade element momentum code is coupled with the RANS solver for the self propulsion case. A workstation is used for the calculations with mesh sizes up to 2×10^6 elements. Computational uncertainty is typically 2-3% for side force and yaw moment but greater than 15% for resistance. With this mesh motion strategy manoeuvres can be well represented within a practical computational time scale.

2 INTRODUCTION

Traditionally the hydrodynamic derivatives for vessels are derived from a combination of towing tank experiments, such as: yawed resistance tests, rotating arm experiments and Planar Motion Mechanism (PMM) tests [1] or through the use of empirical formulas. This work investigates the quality of results that can be achieved using a commercial Reynolds Averaged Navier Stokes (RANS) flow solver, ANSYS CFX Version 11 [2]. This work is a contribution to the SIMMAN workshop [3] and compares the results from CFD based methods with captive and free model tests performed by participating towing tanks.

The KRISO Very Large Crude Carrier 2 (KVLCC2), see Table 1, is hull the hullform considered. KVLCC2 was designed by the Korean Institute of Ships and Ocean Engineering (KRISO) and is representative of full boded ships such as tankers, see Figure 1.



Figure 1: KVLCC2 Hull Form

This investigation considers a combination of drift, pure sway PMM tests and self propulsion using steady and unsteady RANS simulations at varying water depths for direct comparison with experimental results generated by INSEAN, [4] and MOERI

[5]. Model tests were performed on a 1/45.7 scale model of the hull form at Insean No. 2 basin (220 m long x 9 m wide x 3.5 depth) and at the MOERI test tank (200m long x 16m wide x 7 deep) on a 1/58.0 scale model.

Table 1: Principal Dimensions of Vessel

Dimension	Full-Scale	INSEAN	MOERI
Scale	1.00	45.714	58.000
L_{pp} (m)	320.0	7.0000	5.5172
B_{wl} (m)	58.0	1.2688	1.0000
D (m)	30.0	0.6563	0.5172
T (m)	20.8	0.4550	0.3586
∇ (m^3)	312622	3.2724	1.6023

The aim of this work is to investigate the trade-off between computational cost and fluid dynamic fidelity required for unsteady ship manoeuvres.

3 BARE HULL DRIFT AND PMM TESTS IN SHALLOW WATER

A series of simulations of drift and PMM tests were analysed for non-dimensional water depths, 1.2, 1.5, 3.0 and 8.3 (non-dimensional water depth is defined as h/T_m where T_m is mean draught and h is the water depth). The tests were performed at a Froude number of 0.064 corresponding to a vessel speed of 7kn full scale and 0.533 m/s model scale, equating to a model scale Reynolds number of 3.7×10^6 . Drift tests were performed at a series of incidence angles from 0° to 8° . PMM tests were performed at a frequency of $0.06 s^{-1}$.

In order to replicate the sway motion produced in the experimental PMM tests the KVLCC2 geometry moves within the domain, deforming the mesh. CFX has an inbuilt 'mesh morphing' model which is used to calculate the new node locations at each time step, while maintaining mesh topology. The model calculates the displacement on each node using a spring analogy method.

Consequently if the mesh surrounding the vehicle is allowed to deform the elements around the vehicle deform. This can quickly lead to poor quality elements if care is not taken. An alternative method is to replicate the motion of the vessel with the fluid domain split into an inner and outer region. The outer domain remains fixed in space while the inner domain containing the hull moves laterally to replicate the motion induced by a PMM. The mesh in the inner sub domain remains locked in position relative to the lateral motion of the vessel. This

prevents deformation of the detailed mesh around the vessel. The mesh in the outer region is coarser with the inner domain accounting for 89% of the volume and 98% of the elements. The outer mesh is deformed due to the motion of the inner region.

In order to allow the underwater mesh structure to be used for simulations with and without the free surface the domain is further split along the free surface to produce 4 regions, See Figure 2.

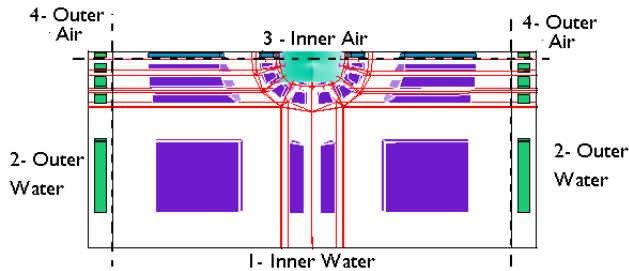


Figure 2: A Cross Section Through the Blocking Structure, Indicating Outer Deformed and Inner Moving Subdomains for Air and Water

4 APPENDED MODEL WITH PROPULSION

Self propelled tests were performed at a model speed of 1.047m/s equating to a Froude number of 0.142 and a Reynolds number of 4.6×10^6 .

The assessment of a ship's manoeuvring performance requires prediction of the forces and moments generated by the rudder. By placing the rudder downstream of the propeller at the aft of the hull the flow is dependent on the three way interaction of the hull, propeller and rudder. While travelling at a drift angle the action of the hull and propeller is to straighten the flow onto the rudder, leading to a decrease in the effective inflow angle to the rudder[6, 7]. Thus to accurately predict the forces acting on the rudder the influence of the hull and propeller on the rudder must be considered.

The model was fitted with a propeller and a semi-balanced rudder based on a NACA0018 section with an area of $0.0654m^2$ and a geometric aspect ratio of 0.55. Table 2 details the propeller properties.

Table 2: Principle Dimensions of Full and Model Scale Vessel

Dimension	Full-Scale	MOERI
TYPE	FP	FP
No. Blades	4	4
D (m)	9.86	0.170
P/D (0.7R)	0.721	0.721
A_e/A_o	0.431	0.431
Rotation	Right Hand	Right Hand
Hub Ratio	0.155	0.155

Numerous studies have used simplified propeller

models to ease simulations of the flow around ships and submarines, see for example [8, 9, 10].

In this work to reduce the computational cost associated with the modelling of the full propeller, the CFD simulation of the flow round the hull is coupled with an external Blade Element Momentum (BEM) [11] code to establish the forces generated by the propeller. These forces are then simulated in the RANS simulations as a series of momentum sources $[f_x, f_y, f_z]$ which are distributed over a cylindrical sub domain enclosing the propeller.

User Fortran modules are used to extract the inflow properties for the propeller from the RANS simulation. During the initial phase of the RANS simulation when the rpm of the propeller is set to zero. The local nominal wake fraction is determined at a series of radial slices (dr) at the inlet to the propeller sub domain by calculating the average circumferential mean velocity.

BEM analysis is used to calculate the thrust (δK_T) and torque (δK_Q) for 10 radial divisions from hub to tip along the propeller blade. The local forces and moments derived by the BEM code are then converted to axial and circumferential momentum sources distributed over the propeller disc.

Figure 3 compares the given open water performance of the MOERI propeller with the performance predicted by BEM theory.

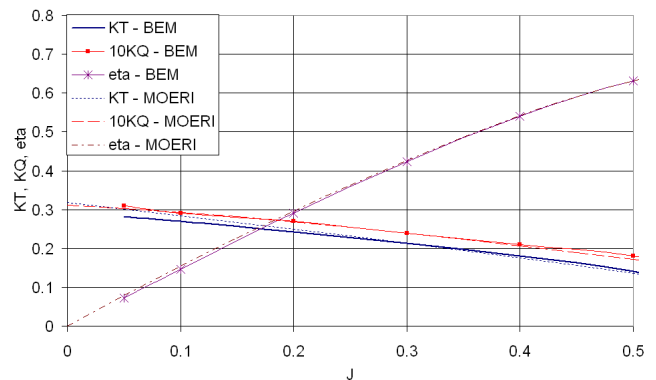


Figure 3: Comparison of Propeller Characteristics For the effective advance speed of interest for this work (nominal $J \sim 0.35$) the agreement is excellent with the variation less than 1%.

The use of a propeller model removes the circumferential variation in loading due to transient and geometric effects. The mean integrated flow is well reproduced to allow hull, propeller and rudder interaction to be simulated, see Figure 4.

5 CFD SIMULATIONS

The fluid flow around the KVLCC2 has been modelled using the commercial finite volume code AN-

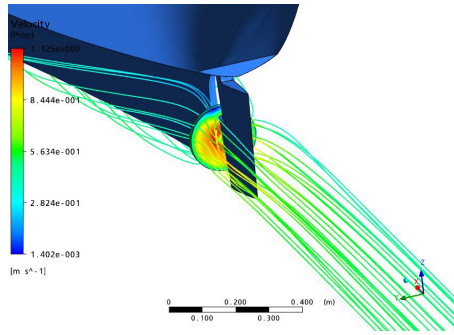


Figure 4: Propeller Model

SYS CFX 11 (CFX) [2]. For these calculations the fluid's motion is modelled using the incompressible (1), isothermal RANS equations (2) in order to determine the cartesian flow field ($u_i = u, v, w$) and pressure (p) of the water around the hull:

$$\frac{\partial \bar{U}_i}{\partial x_1} = 0 \quad (1)$$

$$\frac{\partial \bar{U}_i}{\partial t} + \frac{\partial \bar{U}_i \bar{U}_j}{\partial x_j} = -\frac{1}{\rho} \frac{\partial P}{\partial x_i} + \frac{\partial}{\partial x_j} \left\{ \nu \left(\frac{\partial \bar{U}_i}{\partial x_j} + \frac{\partial \bar{U}_j}{\partial x_i} \right) \right\} - \frac{\partial \bar{u}'_i \bar{u}'_j}{\partial x_j} + f_i \quad (2)$$

In order to maximise the number of cases that could be considered most simulations have been performed assuming a flat free surface. For a few cases a coupled-implicit Volume of Fluid (VOF) algorithm is used to consider the influence of free surface [12]. Details of the computational model are presented in Table 3.

Table 3: Computational model

Parameter	Setting
Turbulence Model	Shear Stress Transport [13]
Multiphase Model	Homogeneous Coupled VOF
Spatial Discretisation	High Resolution
Time Discretisation	2 nd Order Backward Euler
Convergence Control	RMS residual < 10 ⁻⁵

5.1 Mesh Definition

Brogali et al. [14] used an in-house CFD code to investigate the blockage effects during PMM tests of the KVLCC2 in three different width model basins. The influence of tank walls on the calculated derivatives was clearly identified, consequently for these simulations the transverse domain size is selected to match the size of the tank.

For the bare hull configuration a structured mesh is relatively easy to produce and allows rapid creation of multiple meshes. For the appended case creating a suitable blocking structure around the propeller and rudder becomes more complex and an unstructured approach has been used.

All meshes are produced in ANSYS ICEM version 11 [15]. The meshes have been built with a first element thickness equating to a $y^+ \sim 30$, with 10 to 15 elements in the boundary layer.

5.2 Boundary Conditions

To solve the RANS equations a series of boundary conditions are defined. The hull is modelled using a no-slip wall condition. A Dirichlet inlet condition, one body length upstream of the hull is defined where the inlet velocity and turbulence are prescribed explicitly. The model scale velocity is replicated in the CFD analyses; inlet turbulence is set at 5%. A mass flow outlet is positioned downstream of the hull. Three free slip wall conditions are placed at the locations of the floor and sides of the appropriate tank, while the upper boundary is represented by a symmetry plane on the free surface or an opening at deck level if the free surface is considered. The length of the domain was kept small to allow good aspect ratio elements on the free surface.

5.3 Running Simulations

Simulations were run on a high specification desktop pc running 64 bit Windows XP using an AMD Athalon 60 X2 Dual Core Processor 5000+ (2.61GHZ) with 4 GB of RAM. The residual mass error was reduced by four orders of magnitude and lift and drag forces on the hull were monitored to ensure convergence.

For the transient simulations initial steady state simulations are performed to provide initial conditions to the transient simulation. Transient motion simulations are then performed for 1.5 cycles. The first half cycle allows the system to settle before measurement of the derivatives are made over a complete cycle.

6 INDEPENDENCE STUDIES

6.1 Mesh Sensitivity

Two mesh sensitivity studies were performed, one for each meshing strategy. The mesh sensitivity study is presented for the structured meshes for the drift and PMM tests in shallow water at a drift angle of 0° and 6°, see Table 4.

The variation in the global results between the four meshes is small (< 1.5%). This study is predominantly interested in the prediction of sideforce and yaw moment to accurately derive hydrodynamic derivatives. These parameters can be derived without detailed flow information and so the medium mesh was selected for the shallow water cases.

Table 5 gives a mesh sensitivity is given for the self propelled case with the rudder at 10° using a refinement ratio of $r_k = \sqrt{2}$ with the finest mesh having 2x10⁶ elements. Uncertainty assessment has been performed using the methodology presented by Stern et al. [16].

Previous workshops [17, 18] highlight the difficulties in accurate prediction of straight line resistance, with

Table 4: Mesh Sensitivity - Shallow Water Mesh $h/T_m=8.3$

Drift Angle (deg)	Mesh	Nos Elements	Run time (min)	X (N)	Y (N)	N (Nm)
0	Coarse	359999	26	-8.101	0.0303	-0.055
0	Medium	681170	48	-8.029	0.007	-0.027
0	Fine	1325112	102	-7.984	0.009	-0.022
0	Very Fine	1961000	150	-7.984	0.011	-0.024
6	Coarse	359999	34	-9.451	10.900	48.670
6	Medium	681170	48	-9.371	10.880	48.460
6	Fine	1325112	108	-9.322	10.830	48.572
6	Very Fine	1961000	168	-9.323	0.018	48.571

Table 5: Uncertainty Analysis - Self Propulsion Mesh Rudder at 10°

	Exp. (D)	Fine (S_G)	Medium	Coarse	U_G (% S_G)	E (%D)	U_v (%D)
Longitudinal Force, X (N)	-11.05	-11.74	-12.60	-13.82	17.50	-6.28	18.77
Transverse Force, Y (N)	6.79	7.60	7.51	7.33	1.35	-11.89	2.92
Yaw Moment, N (Nm)	-19.47	-18.75	-18.70	-18.35	0.49	3.70	2.54
Thrust, T (N)	10.46	12.53	12.37	12.08	1.57	-19.79	3.13
Rudder X Force, Rx (N)	-2.02	-1.83	-1.89	-1.94	27.83	9.39	25.34
Rudder Y Force, Ry (N)	4.32	4.94	4.99	4.88	1.23	-14.49	2.87

large uncertainty and comparison errors common between calculated and experimental drag unless larger meshes (10M+ elements) are used. self propelled cases where only performed as steady state simulations, hence the finer mesh was used.

6.2 Time Step Sensitivity

Determining an appropriate time step for transient simulations is necessary to ensure valid results while minimising the total run time. There is significant variation in the number of time steps per oscillation used within the literature. To investigate the effect simulations with 50, 100 and 500 time steps per oscillation were performed, corresponding to a Courant number of 7, 3.5 and 0.7.

Results for the variation in sway force are illustrated in Figure 5. For all three cases instabilities are observed during the initial stages of the transient simulation, however, the variation of sway force and yaw moment have stabilised after less than quarter of an oscillation.

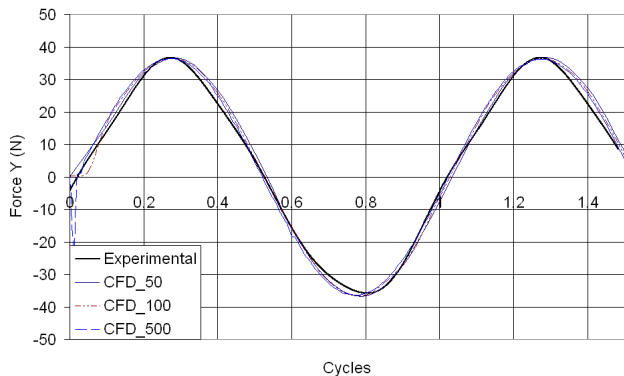


Figure 5: Variation in Predicted Sway Force with Varying Timesteps

7 RESULTS

The results are non-dimensionalised by the length of the vehicle (L) the velocity of the vehicle (V) and the density of the fluid (ρ), a prime symbol is used to signify the non dimensional form for example:

$$v' = \frac{v}{V}, Y' = \frac{Y}{1/2\rho L^2 V^2}, N' = \frac{N}{1/2\rho L^3 V^2} \quad (3)$$

The matching set of experiments were performed with the vessel restrained in roll but free to heave and pitch, however, to reduce simulation time the CFD simulations have assumed the vessel is fixed in heave and pitch at the quoted mean draught and level keel.

7.1 Bare Hull Drift and PMM Tests in Shallow Water

Results are presented for a medium mesh of 700,000 elements. The Froude number (0.064) for the model tests is small consequently unless stated the results do not include free surface effects. The free surface simulations typically increase computational cost by 1000% runtime to allow the wave pattern to develop.

When operating in shallow water the water velocity around the ship is accelerated due to the restriction created by the seabed, see Fig 6. This results in larger forces and moments acting on the vessel.

Figure 7 shows how the depth influences the flow pattern around the hull at a 6° drift angle, although the meshes are not fine enough to completely resolve the vortex structures. For the shallow water case there are two distinct vortex structures forming around the hull, one which separates from the bilge at the forward shoulder on the pressure side and one which separates at the aft end of the bilge. The forward vortex structure is not present in the deep water case and the aft vortex remains attached until

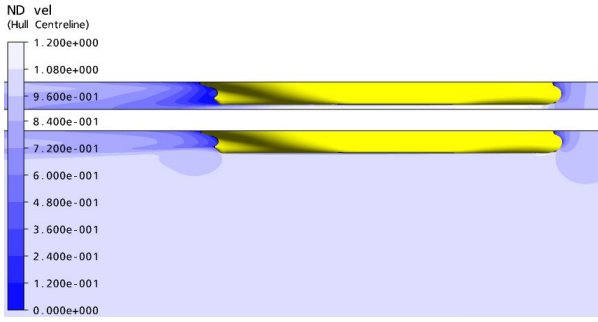


Figure 6: U/U_0 along hull centreline for $H/T_m = 1.2$ (top) and $H/T_m = 8.3$ at 0° drift (bottom)

it reaches the discontinuity at the propeller.

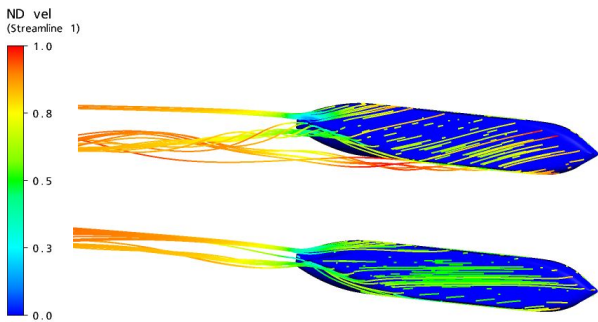


Figure 7: U/U_0 velocity streamlines $H/T_m = 1.2$ (top) and $H/T_m = 8.3$ at 6° drift (bottom)

7.1.1 Prediction of hydrodynamic Derivatives; The results for sway force and yaw moment show good agreement with the experiments over the range of drift angles considered. The simulations performed with the free surface show no significant variation to those performed without at this low Froude number. The CFD simulations predict well the straight line resistance although they fail to accurately predict the induced drag component when the hull is travelling at a drift angle.

The predicted hydrodynamic derivatives are compared in Table 6. The correlation between model tests and CFD for all but the shallowest case are very good, with less than 10% discrepancy. For the very shallow water case the results are less close however the trends are still captured. The most likely cause of the shallow water discrepancy is the use of a fixed model, while in the experiment the vessel was free to squat.

7.1.2 Pure Sway PMM; The predicted surge and sway forces and yaw moments from the CFD simulation for pure sway PMM simulations are compared with experimental results in Figures 8 and 9.

The maximum sway force and yaw moment are well predicted while the variation in the drag force predicted by CFD is very small, the experimental variation is large, however, the mean force is well captured. Again the correlation between experiential and CFD simulations is best in deeper water.

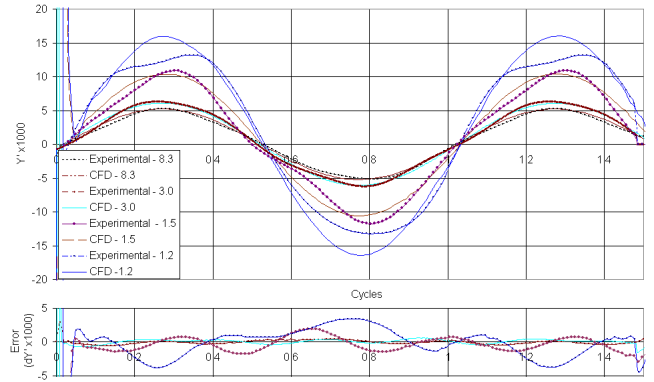


Figure 8: Variation of Sway Force During Pure Sway PMM Test

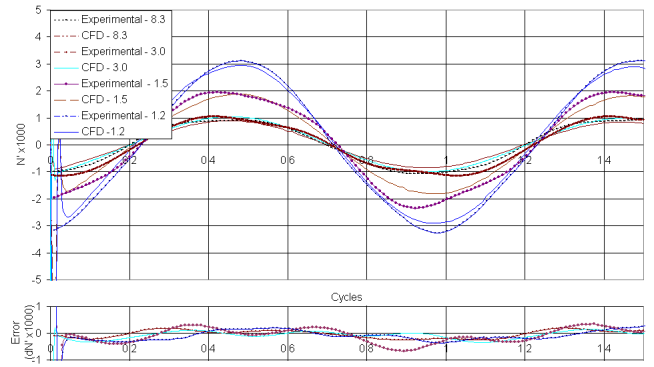


Figure 9: Variation of Yaw Moment During Pure Sway PMM Test

7.2 Appended Model with Propulsion

The 1/58 scale model fitted with the propeller operating at $n=8.59$ rps was tested at a series of drift and rudder angles. Figures 10 illustrate the variation of global forces with variation in drift angle. The influence of drift angle on global loads is well captured even at larger amplitude drift angles outside the linear region.

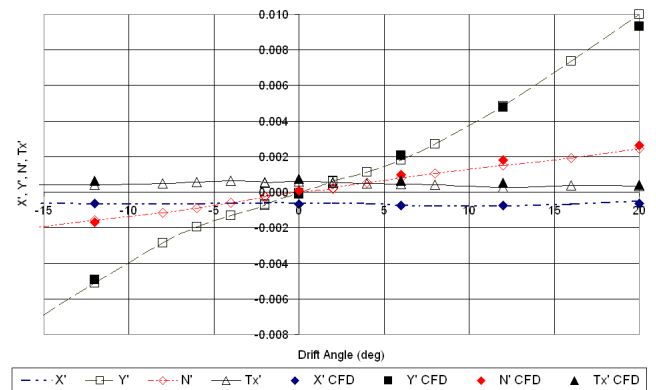


Figure 10: Influence of Drift Angle on Force Coefficients at a Model speed of 1.047m/s

Prediction of the rudder forces is dependent on the rudder inflow conditions which are dominated by the action of the hull and the propeller. Thus to accurately capture the rudder forces the flow in the stern

Table 6: Hydrodynamic Derivatives

h/T_m	$Y'v$			$N'v$		
	Exp.	CFD	E[%Exp.]	Exp.	CFD	E[%Exp.]
1.2	0.0423	0.0473	11	0.0160	0.0189	15
1.5	0.0237	0.0252	6	0.0108	0.0110	2
3.0	0.0111	0.0107	-4	0.0066	0.0060	-10
8.3	0.0081	0.0079	-3	0.0053	0.0051	-4

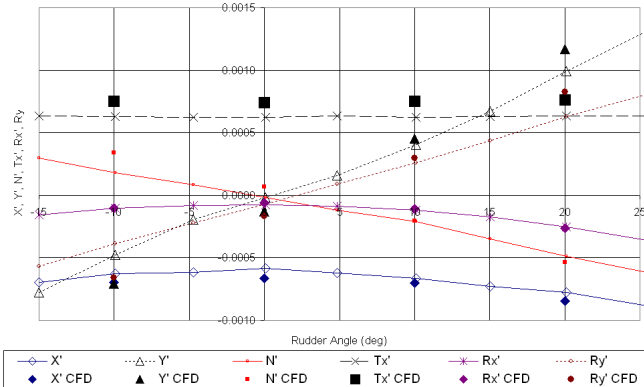


Figure 11: Influence of Rudder Angle on Force Coefficients at a Model speed of 1.047m/s

of the vessel needs to be captured with a high level of accuracy, to ensure the correct flow into the propeller and then across the rudder. Small over predictions in the thrust generated by the propeller lead to an increased inflow velocity which leads to significant over prediction of rudder force. This is seen in Figure 11 where the predicted propeller thrust is approximately 20% higher than the experimental result, leading to overproduction of the global sideforce and yawing moment which are dominated by the rudder loads. However the trends are well captured and refinement of the model should lead to better correlation.

8 CONCLUSIONS

The global forces and moments acting on the KVLCC2 hull undergoing a series of steady and unsteady maneuvers has been investigated using CFD.

Drift and PMM tests were replicated in a range of water depths for the unappended hull, with good agreement between experimental and CFD simulations for all but the shallowest water case. The application of a moving body fitted inner domain with a fixed outer domain was shown to work well.

The CFD simulation was coupled with an external blade element momentum code to simulate the propeller action. CFD simulations are able to predict the global forces and moments acting on a vessel undergoing steady drift with a good level of accuracy.

A mesh density of 2M cells proves inadequate for self propulsion and propeller design calculations. In particular the rudder mesh detail was insufficient, either

a finer mesh or alternative modelling methods are required to better capture its influence. A good level of understanding of the global forces and moments can be obtained with this mesh resolution for use in manoeuvring calculations based on a workstation computer, at a practical computational cost.

REFERENCES

- [1] J. P. Constock. *Principles of Naval Architecture*. SNAME, 1967.
- [2] CFX. *CFX Manual*. ANSYS, 2005.
- [3] *SIMMAN Website*. World Wide Web, <http://www.simman2007.dk/>, 2007.
- [4] *INSEAN Website*. World Wide Web, www.insean.it, 2007.
- [5] *MOERI Website*. World Wide Web, <http://www.moeri.re.kr/eng/index.htm>, 2007.
- [6] A.F. Molland and S. R. Turnock. Flow straightening effects on a ship rudder due to upstream propeller and hull. *Int. Shipbuild. Progr.*, 49:195–214, 2002.
- [7] A.F. Molland and S.R. Turnock. *Marine Rudders and Control Surfaces*. Butterworth-Heinemann, 2007.
- [8] S.B. Mueller, M. Steden, J. Neugebauer, M.F. El-Haddad, and M. Abdel Maksaud. Comparing a propeller model with a rotating propeller in a cfd-simulation of the viscous flow around a ship. In *9th Numerical Towing Tank Symposium, le Croisic*, 2006.
- [9] Y.Nishi, M. Kashiwagi, W. Koterayama, and M. Nakamura. Resistance and propulsion performance of an underwater vehicle estimated by a cfd method and experiment. In *Proceedings of the Seventeenth (2207) International Offshore and Polar Engineering Conference*, 2007.
- [10] K-J Han, L. Larsson, and B. Regenstrom. A rans study on the interaction between a propeller and a rudder in open water. In *10th Numerical Towing Tank Symposium, Hamburg*, 2007.
- [11] A. F. Molland and S. R. Turnock. A compact computational method for predicting forces on a rudder in a propeller slipstream. In *Transactions of RINA*, volume 138, pages 59–71, 1996.
- [12] S. Eder. Free surface flow simulation with a coupled algebraic multigrid algorithm. In *10th Numerical Towing Tank Symposium, Hamburg*, 2007.
- [13] F.R. Menter. Two-equation eddy-viscosity turbulence models for engineering applications. *AIAA Journal*, 32(8):1598 – 605, 1994/08/.
- [14] R. Brogali, R. Muscari, and A. Di Mascio. Numerical analysis of blockage effects in pmm tests. In *In Proc. 26th Symposium on Naval Hydrodynamics Rome, Italy*, 17-22 September 2006.
- [15] ANSYS. *ANSYS ICEM CFD Product Overview*. World Wide Web, <http://www.ansys.com/products/icemcfd.asp>, 2006.
- [16] F.Stern, R. V. Wilson, H. W. Coleman, and E. G. Pateron. Verification and validation of cfd simailatons. Technical Report IIHR Report No. 407, Iowa Institute of Hydraulic Research, September 1999.
- [17] L. Larsson, F. Stern, and V. Bertram. Benchmarking of computational fluid dynamics for ship flows: The gothenburg 2000 workshop. *Journal of Ship Rese*, 47:63–81(19), 1 March 2003.
- [18] T. Hino, editor. *CFD Workshop Tokoyo*. National Maritime Research Institute, March 2005.